Title	In vitro analysis of durability of S-PRG filler-containing composite crowns for primary molar restoration
Author(s)	Nakase, Yutaro; Yamaguchi, Satoshi; Jalkh, Ernesto B.Benalcázar et al.
Citation	Dental Materials. 2023, 39(7), p. 640-647
Version Type	VoR
URL	https://hdl.handle.net/11094/92521
rights	This article is licensed under a Creative Commons Attribution 4.0 International License.
Note	

In vitro analysis of durability of S-PRG filler-containing composite crowns for primary molar restoration

Yutaro Nakase[a,g], Satoshi Yamaguchi[a,*], Ernesto B. Benalcázar Jalkh[b], Pablo J. Atria[c],
Lukasz Witek[d,e,h], Estevam A. Bonfante[b], Hefei Li[a], Takahiko Sakai[a,f], Rena Okawa[g],
Kazuhiko Nakano[g], Satoshi Imazato[a]

[a] *Department of Dental Biomaterials, Osaka University Graduate School of Dentistry, 1-8 Yamadaoka, Suita, Osaka 565–0871, Japan*
[b] *Department of Prosthodontics and Periodontology, Bauru School of Dentistry, University of São Paulo, Bauru, SP, Brazil*
[c] *Department of Biomaterials, College of Dentistry, Universidad de los Andes, Santiago, Chile*
[d] *Biomaterials Division, NYU College of Dentistry, New York, NY, USA*
[e] *Department of Biomedical Engineering, NYU Tandon School of Engineering, Brooklyn, NY USA*
[f] *Department of Fixed Prosthodontics and Orofacial Function, Osaka University Graduate School of Dentistry, 1-8 Yamadaoka, Suita, Osaka 565-0871, Japan*
[g] *Department of Pediatric Dentistry, Osaka University Graduate School of Dentistry, 1-8 Yamadaoka, Suita, Osaka 565-0871, Japan*
[h] *Hansjörg Wyss Department of Plastic Surgery, New York University Grossman School of Medicine, New York, NY, USA*

ARTICLE INFO

ABSTRACT

Objective: To evaluate the reliability, maximum principal stress, shear stress, and crack initiation of a computer-aided design/computer-aided manufacturing (CAD/CAM) resin composite (RC) incorporating surface pre-reacted glass (S-PRG) filler for primary molar teeth.
Methods: Mandibular primary molar crowns fabricated by experimental (EB) or commercially available CAD/CAM RCs (HC) were prepared and cemented to a resinous abutment tooth using an adhesive resin cement (Cem) or a conventional glass-ionomer cement (CX). These specimens were subjected to a single compressive test (n = 5/each) and the step-stress accelerated life testing (SSALT) (n = 12/each). Data was evaluated using Weibull analyses and reliability was calculated. Afterwards, the maximum principal stress and crack initiation point of each crown was analyzed by finite element analysis. To evaluate bonding of EB and HC to dentin, microtensile bond strength (μTBS) testing was conducted using primary molar teeth (n = 10/each).
Results: There was no significant difference between the fracture loads of EB and HC for either cement (*p* > 0.05). The fracture loads of EB-CX and HC-CX were significantly lower than EB-Cem and HC-Cem (*p* < 0.05). The reliability at 600 N for EB-Cem was greater than that for EB-CX, HC-Cem, and HC-CX. The maximum principal stress concentrated on EB was lower than that on HC. The shear stress concentrated in the cement layer for EB-CX was higher than that for HC-CX. There was no significant difference among the μTBSs of EB-Cem, EB-CX, HC-Cem, and HC-CX (*p* > 0.05).
Significance: The crowns fabricated with the experimental CAD/CAM RC incorporating S-PRG filler yielded greater fracture loads and reliability than the crowns manufactured with commercially available CAD/CAM RC regardless of the luting materials. These findings suggest that the experimental CAD/CAM RC crown may be clinically useful for the restoration of primary molars.

1. Introduction

In pediatric dentistry, primary posterior teeth with extensive caries have been restored with ready-made full metal and ceramic crowns owing to their superior mechanical properties over resin composites (RC). Stainless steel crowns (SSCs) were introduced into pediatric dentistry in 1950, and are considered as one of the most effective restorations for long-term success [1]. However, because of their non-aesthetic appearance [2], parents may prefer to avoid SSC restoration in their children.

In a previous study, our group developed novel experimental CAD/CAM RC incorporating surface pre-reacted glass (S-PRG) filler for primary teeth crowns [3]. Such composite demonstrated promising physical properties and wear resistance, with greater fracture toughness and wear resistance regarding a commercially available CAD/CAM RC and two resin composites for primary teeth [3]. While the evaluation of fundamental properties provide valuable information on materials behavior, the long-term clinical reliability (probability of survival) of dental restorative materials depends on its performance under cyclic loading and wet environments, which have a significant impact on crack propagation and failure, and correlates more closely to clinical scenarios [4].

As the luting material, conventional glass-ionomer cement (GIC), a less technique-sensitive material commonly used for stainless steel crowns cementation, might be of interest for clinical application as luting agent for CAD/CAM RC crowns. The experimental CAD/CAM RC incorporate S-PRG filler, which has a pre-reacted glass-ionomer phase containing F$^-$, Al^{3+}, BO$_3$$^{3-}$, Na$^+$, SiO$_4$$^{4-}$, or Sr^{2+} on its surface [5]. In this regard, an adhesion via the ionic/coordinate bond between Sr^{2+}/Al^{3+} on the S-PRG filler, which is exposed on the inner surface of the CAD/CAM RC crown, and the carboxylate ions in the polyacrylic acid of GIC is expectable.

Although fatigue testing of anatomic samples has been used to predict the clinical performance of permanent RC crowns, [6] there are no reports evaluating the probability of survival of primary teeth crown-shaped specimens. Considering the significant differences in the anatomy and amount of tooth preparation required for primary and permanent crowns [7,8], it is questionable whether CAD/CAM RC crowns will present an acceptable performance as a restorative material for primary teeth restorations. Thus, the aim of this study was to evaluate the reliability of the previously developed CAD/CAM RC crowns incorporating S-PRG filler for primary molars compared to commercially available CAD/CAM RC. Also, the bonding of experimental CAD/CAM RC crown to dentin was evaluated by microtensile bond strength test using a resin cement and a conventional GIC.

2. Materials and medthods

2.1. CAD/CAM RCs and luting materials

An experimental CAD/CAM RC (EB) [3] and a commercially available CAD/CAM RC (Shofu Block HC, Shofu, Kyoto, Japan; HC) were used (Table 1). For luting, a commercially available resin cement (Block HC Cem, Shofu; Cem), and a conventional glass-ionomer cement (HY-BOND GLASIONOMER CX, Shofu; CX) were employed (Table 2).

2.2. Specimen preparation

An impression of a mandibular primary second molar abutment (D5D-407 C, Nissin, Kyoto, Japan) was taken using a polyvinyl siloxane

impression material (Exafine Putty type, GC, Tokyo, Japan). A total of 68 abutment teeth were fabricated by incremental build-up and photopolymerization of the core resin (Unicast, GC) in the impression cavity. The mandibular right second primary molar model (A5A-500, Nissin) and the abutment were scanned (Shofu S-WAVE scanner D2000, Shofu) and designed (Dental System 2016, Shofu). The abutment tooth was prepared with a 0.8-mm chamfer width, minimal occlusal reduction of 1.0 mm by a certified specialist of the Japanese Society of Pediatric Dentistry. Both models were fabricated using a milling machine (DWX-50, Kuraray Noritake Dental, Tokyo, Japan). To strengthen the adhesion, their inner surface of the crowns was sandblasted with an air pressure at 0.2 MPa using Al$_2$O$_3$ particles (diameter: 30–50 μm) [20]. Subsequently, the samples were ultrasonic cleaned and air-dried for 10 s. A mixture of two primers (Primer A + Primer B) was applied to the abutment and after 20 s, a resin primer (HC Primer, Shofu) was applied to the inner surface of each crown (HC-Cem and EB-Cem groups). The crowns were cemented on the abutment tooth and photopolymerized at 2000 mW/cm^2 for 20 s followed by removing any excess cement. For the groups cemented with glass-ionomer (HC-CX and EB-CX groups), a liquid-powder mixture on a ratio of 1:2 was prepared and applied to the inner surface of each crown. Crowns were placed onto the abutments followed by removing any excess cement.

2.3. Single compressive testing and analysis

All specimens were vertically embedded in a 25-mm diameter polyvinyl chloride (PVC) tube with acrylic resin (Ortho-Jet, GC) with the margins of the crown positioned 2 mm above the surface of the acrylic resin. Samples were stored in distilled water at 37 ℃ for 24 h. A compressive single load to failure test (INSTRON 5566, Shimadzu, Kyoto, Japan) was conducted at a crosshead speed of 0.5 mm/min (n = 5) until failure. The maximum load at fracture was recorded for each sample and the mean fracture load and standard deviation were calculated. Based on the results of the compressive test, three loading profiles were designed for fatigue testing as described in the correspondent section. The fractured specimens were observed with stereomicroscopy (SMZ-745 T, Nikon, Tokyo, Japan) using high dynamic range software (NIS-Elements Ver.4.0, Nikon).

Finite element analysis models of the indenter, crown, cement, abutment tooth, and acrylic resin base were designed by using pre- and postprocessor (LS-PrePost, ANSYS, Pennsylvania, USA) based on the scanned stereolithography (STL) data (Supplementary Fig. 1) of the *in vitro* tests. The bottom surface of acrylic resin base was fixed. Axial displacements (1.0 mm) along to the tooth axis were applied to the occlusal surface of the crown by the indenter. The fracture initiation point, maximum principal stress distribution of the crown, shear stress distribution of the cement layer were analyzed. The number of elements for the indenter, crown, cement, abutment tooth and resin base were 9216, 88,816, 19,661, 169,725, and 78,491, respectively. The elastic moduli and fracture strains of the CAD/CAM RCs and cements were determined according to the *in vitro/in silico*

Table 1

Material compositions of computer-aided design/computer-aided manufacturing resin composites used in this study.

Materials	Code	Filler	Monomer	Filler content (wt %/vol%)	Average particle size of filler (μm)	Manufacturer
Experimental CAD/CAM RCB containing S-PRG filler	EB	S-PRG filler, Multi-functional glass filler	Bis-GMA, Bis-MPEPP, TEGDMA	63.4/41.7	0.4	Shofu, Japan
Shofu Block HC	HC	Silica filler, Zirconium silicate, Micro fumed silica	UDMA, TEGDMA	68.0/52.0	2–15 1–10 0.01–0.04	Shofu, Japan

Surface pre-reacted glass (S-PRG) filler: the filler having three layer structure developed by applying PRG technology (forming a glass-ionomer phase only on the surface of a glass core layer by means of an acid-base reaction between special surface-treated multi-functional fluoroboroaluminosilicate glass filler and poly-carboxylic acid in the presence of water), Multi-functional glass filler: special surface-treated fluoroboroaluminosilicate glass filler, Bis-GMA: Bisphenol A-diglycidyl methacrylate, Bis-MPEPP: 2,2-bis(4-methacryloxypolyethoxyphenyl)propane, TEGDMA: Triethyleneglycol Dimethacrylate

Table 2
Material compositions of resin cements used in this study.

Materials	Code	Component	Manufacturer
Block HC Cem	Cem	A paste: UDMA, S-PRG filler, Silicate glass, Photo polymerization initiator, Chemical polymerization initiator and others B paste: UDMA, 2-HEMA, Carboxylic acid monomer, Phosphonic acid monomer, Chemical polymerization initiator, Photo polymerization initiator and others	Shofu, Japan
HC primer		UDMA, MMA, Acetone, Photo polymerization initiator, Chemical polymerization initiator and others	
Primer A/B		A primer: Water, Acetone, Chemical polymerization initiator and others B primer: 2-HEMA, Carboxylic acid monomer, Acetone and others	
HY-Bond Glassionomer CX	CX	Powder: Fluoroalminosilicate glass, HY agent, pigments Liquid: Acrylic acid tricarboxylic acid co-polymer solution, Tartaric acid	Shofu, Japan

UDMA: urethane dimethacrylate, S-PRG filler: surface pre-reacted glass filler, 2-HEMA: 2-hydroxyethyl methacrylate, MMA: methyl methacrylate, HY agent: tannin-fluoride additive

Table 3
Material properties used for finite element analysis. SIGP1 is failure criteria of maximum principal stress according to fracture strain.

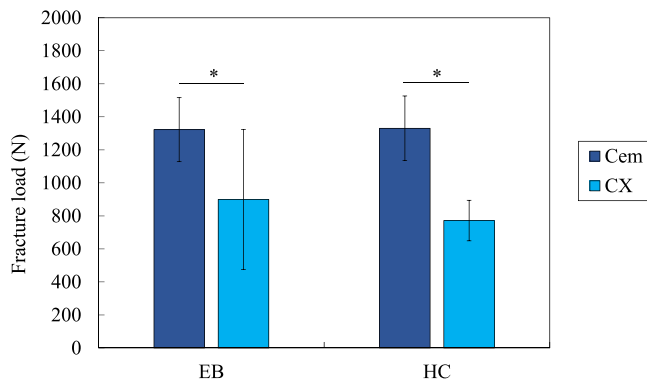|	Elastic modulus (MPa)	Density (g/cm^3)	Fracture strain	SIGP1 (MPa)
EB	5200	1.88	0.0180	76.3
HC	6800	1.64	0.0215	128.9
CX	4000	2.26	0.0029	12.4
RC	2500	1.84	0.0166	61.0

Fig. 1. Fracture loads after the *in vitro* single compressive test for each specimen. The asterisk indicates a significant difference ($p < 0.05$).

three-point bending test [9,10]. *In silico* three-point bending analysis was repeatedly performed by using non-linear dynamic FEA (LS-DYNA, ANSYS, Pennsylvania, USA) by changing the elastic modulus. When the root mean squared error of the load in the *in vitro* and *in silico* load–displacement curve was less than 1 N, the arbitrary elastic modulus was determined as the true elastic modulus of the material [9]. The density of the CAD/CAM RCs and cements was calculated by the volume, obtained from micro-computed tomography (micro-CT; R_mCT2, Rigaku, Tokyo, Japan), and respective weight of each material. All analyses were conducted using the dynamic explicit method. The crown, cement, abutment tooth, and resin base were defined as the piecewise linear plastic material (MAT_024) using the effective stress-strain curve according to each material. The indenter was defined as the rigid material (MAT_20). Material properties used for finite element analysis were summarized in Table 3. The Poisson's ratio of each material was set to 0.38 according to that of polymers. The resin base was assumed as a rigid body (no deformation).

2.4. Microtensile bond strength test

The first primary molar teeth (upper and lower) used were collected upon receiving approval from the Institutional Review Board of Osaka University Dental Hospital (IRB No. H29-E28). Each tooth´s dentin surface was exposed using a low-speed saw (Isomet; Buehler, Illinois, USA) under water irrigation. Rectangular specimens (4 × 4 × 14 mm) were prepared for HC and EB. A 4 × 4 mm^2 surface area of each specimen was polished with 2000-grid silicon carbide (SiC) paper and cemented using either Cem or CX on the exposed dentin surface according to the same protocol in the Section 2.2. All specimens were stored in distilled water (DI-H$_2$O) at 37 ℃ for 24 h and then bar-shaped specimens with a section area of 1 × 1 mm^2 were prepared. Each specimen was fixed on a jig and a µTBS test [11] (EZ-SX, Shimadzu) was conducted at a crosshead speed of 1.0 mm/min (n = 10/each group). Failure mode was characterized as adhesive, cohesive or mixed.

2.5. Fatigue test

Based on the mean load of the static compression test, three fatigue loading profiles were designed, and 12 specimens per group were submitted to the step-stress accelerated life testing (SSALT) [8]. The profiles were designated as mild (n = 6), moderate (n = 4), and aggressive (n = 2), following a 3:2:1 ratio (Supplementary Fig. 2). The SSALT was conducted at a frequency of 5 Hz with increasing load until failure or suspension using an electrodynamic fatigue testing machine (ELF 3300, EnduraTec Division, Bose Corporation, Minnetonka, MN, USA). For fatigue testing, the samples were immersed in DI-H$_2$O and a semispherical stain steel indenter with 6 mm of diameter was used for load application in three occlusal points to simulate the occlusal contacts of natural primary occlusion (Supplementary Fig. 3). Upon completion of testing, data was subjected to a Weibull analysis and a reliability assessment.

Data analysis consisted of an underlying life distribution to describe the life data collected at different stress levels and a life-stress relationship to quantify the manner in which the life distribution changed across different stress levels. Therefore, the Weibull Distribution was chosen to fit the life data collected in SSALT. Considering the time-varying stress model, the inverse power law relationship was selected to extrapolate a use level condition considering a cumulative damage model. Parameters estimation for all analyses was accomplished via Most Likelihood Method, and 90% two-sided confidence interval was approximated using the Fisher matrix approach. Hence, the use level probability Weibull curves (probability of failure versus number of cycles) with a set load of 600 N (highest load used for reliability analysis) were calculated and plotted (Synthesis 9, Alta Pro, Reliasoft, Tucson, AZ, USA). Reliability assessment was performed for given missions at 200, 400 and 600 N for 100,000 cycles with analysis of correspondent 90% confidence intervals.

Qualitative evaluation of the fractured specimens was observed using scanning electron microscopy (SEM; JSM-6390BU, JEOL, Tokyo, Japan) at 20 × magnification and 5 kV.
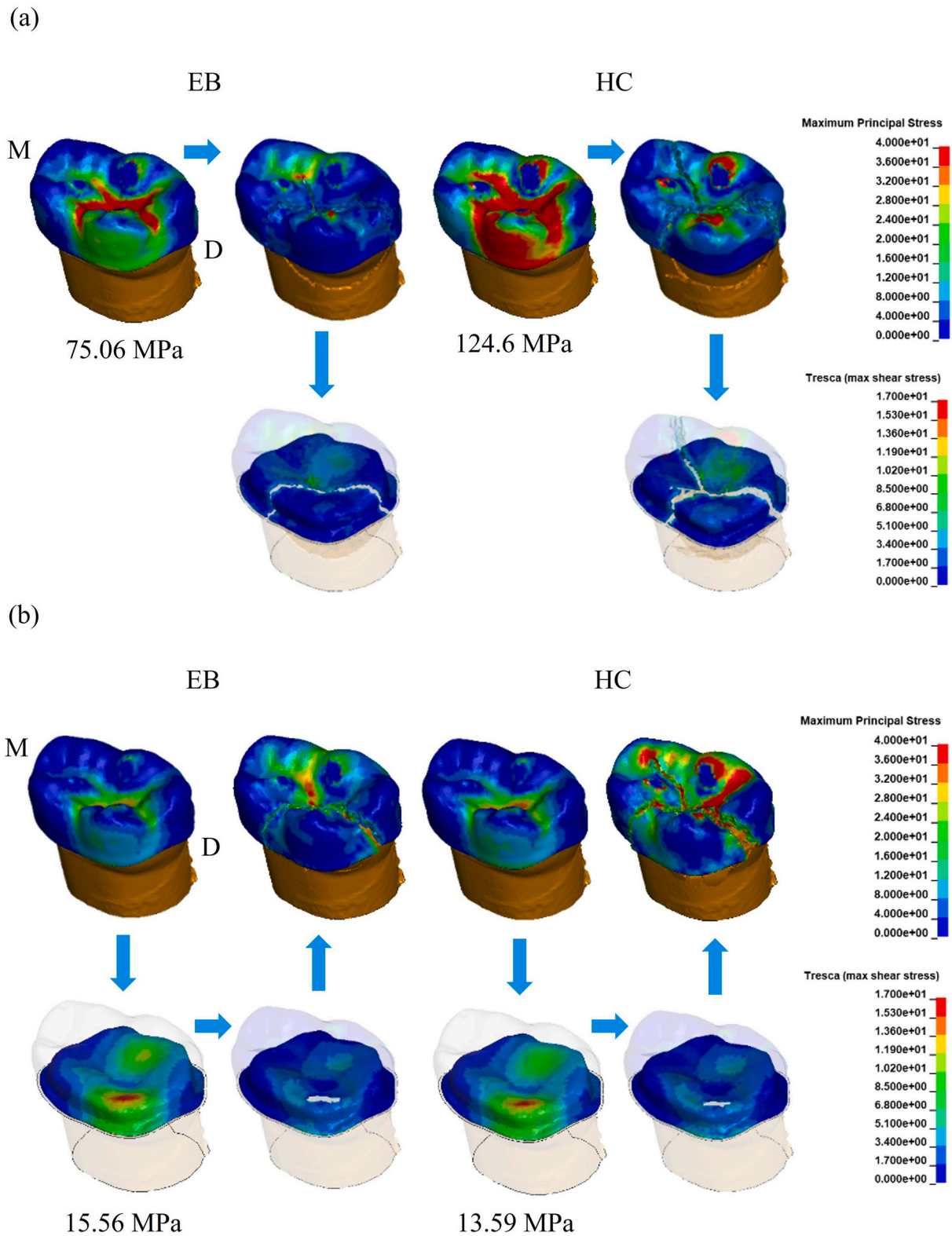
Fig. 2. Maximum principal stress or shear stress distribution in computer-aided design/computer-aided manufacturing resin composite crown for primary molar teeth or adult teeth bonded by (a) resin cement or (b) conventional glass-ionomer cement on a resinous abutment obtained by *in silico* non-linear dynamic finite element analysis. M: mesial, D: distal.

2.6. Statistical analysis

The mean and standard deviation of the fracture loads were analyzed using two-way analysis of variance (ANOVA). The mean and standard deviation of the μTBSs were analyzed with one-way ANOVA and the Tukey's honest significant difference (HSD) test (PASW Statistics 25, IBM, Somers, NY, USA). P-values of less than 0.05 were considered as statistically significant.
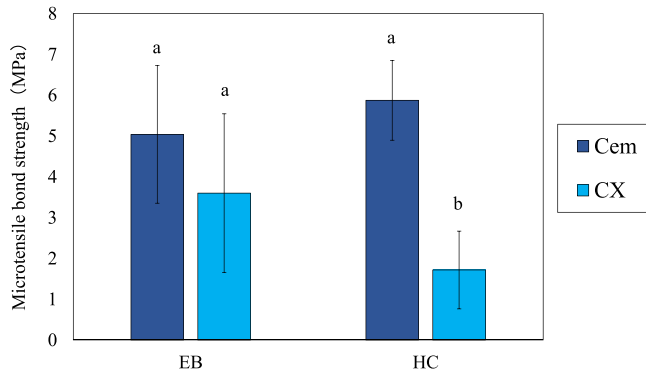
Fig. 3. Microtensile bond strengths of each specimen.

Table 4

Failure modes after microtensile bonding test [A/B]. Numbers in square brackets are the number of specimens classified into two failure modes [A/B]: [A] adhesive failure along the cement–CAD/CAM resin composite interface; [B] mixed failure between the cement and CAD/CAM resin composite.

	Cem	CX
EB	[3/7]	[2/8]
HC	[3/7]	[7/3]

3. Results

3.1. Fracture loads

The fracture load of EB-CX (899 $\pm$ 425 N) were significantly lower than that of EB-Cem (1322 $\pm$ 194 N) ($p < 0.05$) (Fig. 1). The fracture load of HC-CX (772 $\pm$ 123 N) was also significantly lower than that of HC-Cem (1331 $\pm$ 196 N) ($p < 0.05$). There was no significant difference detected between the fracture loads of EB-Cem (1322 $\pm$ 194 N) and HC-Cem (1331 $\pm$ 196 N) ($p > 0.05$), or EB-CX (899 $\pm$ 425 N) and HC-CX (772 $\pm$ 123 N) ($p > 0.05$). EB-Cem and HC-Cem fractured without debonding from the abutment tooth (Supplementary Fig. 4a and Supplementary Fig. 4b). Further, residual cement was observed in the inner surface of EB-CX (Supplementary Fig. 4c), while it was absent in the inner surface of HC-CX (Supplementary Fig. 4d). An initial load of the three profiles for the SSALT was determined from ~8% of the mean fracture load of 1081 N (i.e. 80 N).

3.2. Crack initiation point and stress concentration

Fig. 2 shows the crack initiation points and maximum principal/shear stress distribution obtained from the *in silico* compression analysis. The crack initiation point was observed around the distobuccal cusp for EB-Cem and HC-Cem (Fig. 2a) whereas at the cement layer for EB-CX and HC-CX (Fig. 2b). The shear stress concentrated in the cement layer for EB-CX was higher than that for HC-CX.

3.3. Microtensile bond strength and failure mode

There was no significant difference in the microtensile bond strength mean values among EB-Cem, EB-CX, and HC-Cem ($p > 0.05$) (Fig. 3). The microtensile bond strength of HC-CX was significantly lower than that of EB-CX and HC-Cem ($p < 0.05$) (Fig. 3). The failure modes after the microtensile bonding test are summarized in Table 4. As for the EB-Cem and HC-Cem, mixed failure was observed between the CAD/CAM RC crown and cement. For HC-CX and EB-CX, adhesive failure along the crown-cement interface and mixed failure were observed, respectively.

3.4. Fatigue performance

Fig. 4 shows SEM images of fractured specimens after the SSALT. Crack initiation points of EB-Cem and HC-Cem was observed at the outer surface of crown (Fig. 4a and Fig. 4b) while the those of EB-CX and HC-CX were observed at the inner surface of crown (Fig. 4c and
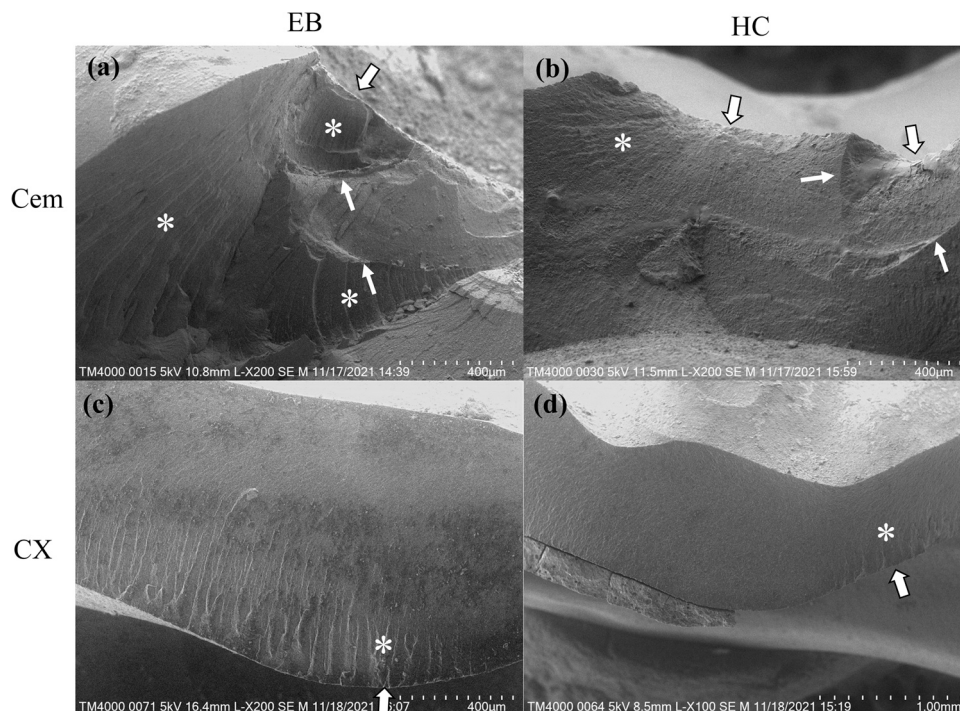

Fig. 4. Scanning microscopic images observed from each fractured specimen after step-stress accelerated life test. Large white arrows indicate crack initiation points. Arrested lines are indicated by small white arrows. Hackle patterns following the direction of crack propagation are indicated by asterisks.
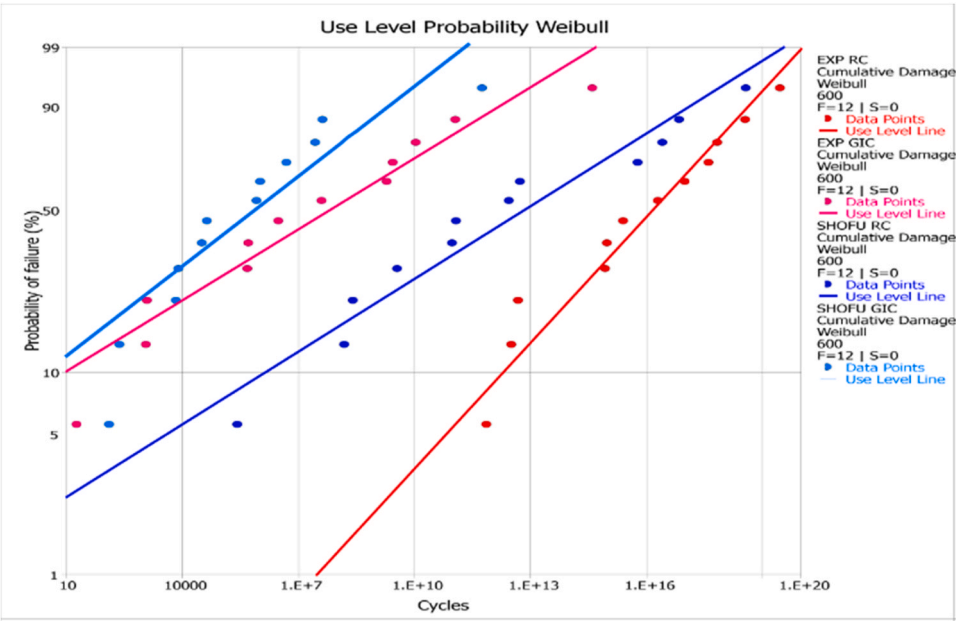
Fig. 5. Probability of failure (%) obtained from each specimen after the step-stress accelerated life test.

Table 5
Weibull parameters and 90% confidence bounds of all experimental groups.

	EB		HC	
	Cem	CX	Cem	CX
upper	1527.76	892.46	1394.54	998.39
Characteristic Strength	1423.77 [A]	812.84[B]	1241.79 [A]	850.78[B]
lower	1326.88	740.32	1105.77	724.99
upper	10.42	7.74	6.30	4.41
Weibull Modulus	7.10 [A]	5.38 [A]	4.33 [A]	3.16 [A]
lower	4.84	3.74	2.98	2.26

There was no significant difference among same letters.

Table 6
Reliability at 100,000 cycles for missions at 200, 400 and 600 N after step-stress accelerated testing.

		200 N	400 N	600 N
EB	Cem	100(99–100)[aA]	99(99–100)[aA]	99(96–99)[aA]
	CX	99(98–99)[aA]	96(85–99)[abAB]	72(50–85)[bBC]
HC	Cem	99(98–99)[aA]	99(98–99)[aA]	92(76–97)[bAC]
	CX	98(91–99)[aA]	94(68–95)[abB]	59(37–75)[bB]

There was no significant difference among same letters.

Fig. 4d). The probability of failure Weibull plot obtained from SSALT is presented in Fig. 5 and Weibull parameters along with 90% CIs are summarized in Table 5. Weibull configuration factor β (two-sided at 90% confidence intervals (CI)) for EB-Cem, EB-CX, HC-Cem, and HC-CX were 0.211 (CI: 0.115–0.389), 0.119 (CI: 0.067–0.214), 0.122 (CI: 0.05–0.298), and 0.148 (CI: 0.086–0.256), respectively. The shape parameter m (two-sided at 90% confidence intervals: CI) for EB-Cem, EB-CX, HC-Cem, and HC-CX were 7.099 (CI: 4.835–10.422), 5.383 (CI: 3.744–7.738), 4.331 (CI: 2.977–6.301), and 3.16 (CI: 2.263–4.413), respectively. The scale parameter η (two-sided at 90% confidence bounds) for EB-Cem, EB-CX, HC-Cem, and HC-CX were 1423.77 (CI: 1326.87–1527.75), 812.83 (CI: 740.31–892.45), 1241.78 (CI: 1105.76–1394.54), and 850.77 (CI: 724.99–998.38), respectively. A greater reliability for completion of mission of 200 N, 400 N, and 600 N at 100,000 cycles was recorded for EB-Cem (100%, 99%, and 99%) than HC-Cem (99%, 99%, and 92%), EB-CX (99%, 96%, and 72%), and HC-CX (98%, 95%, and 59%). The reliability for completion of mission at 400 N and 600 N at 100,000 cycles for HC-CX was significantly decreased relative to HC-Cem (Table 6).

4. Discussion

CAD/CAM RC crowns have been clinically used as restorations to replace lost tooth substrate. Upon receiving approval from the Japanese health insurance companies in 2014, CAD/CAM RC crown restorations of premolars and molars have rapidly exceeded those of metals and ceramics [6]. In this study, accelerated fatigue tests of experimental and commercially available CAD/CAM RC primary molar crowns was performed *in vitro,* and the crack initiation points were determined by *in vitro* single compression test and *in silico* compressive analysis.

Single compressive test, the mean fracture load of EB-Cem and EB-CX were 1322 ± 194 N and 899 ± 425, respectively. Both fracture loads exceeded 814 N, which is a mean occlusal load of an adult male [11]. These results suggest that EB has clinically acceptable strength for restoring primary molar teeth. The *in silico* compressive analysis revealed that EB-CX exhibited minimal failure of the crown and the abutment tooth in terms of crack propagation. A lower stress concentration was observed for EB compared to HC in the maximum principal stress distribution in the crown. This stress concentration was due to the lower elastic modulus of EB compared to HC. In terms of the shear stress distribution in the cement layer, a higher stress concentration was observed for CX than Cem. This stress concentration was due to higher deformation of EB than HC. As a result, that crack initiation point was observed from CX due to its lower fracture strain compared to EB, HC, Cem, and abutment tooth. Also, the crack originated from the inner surface of the crown in case of EB-CX, which is consistent with the findings of the fractographic analysis after fatigue testing.

As the luting material, resin cements are generally used for CAD/CAM RCs. However, moisture control can be challenging for most pediatric cases, which may impair adhesive performance of resin cements and compromise the long-term success of the treatment. Therefore, conventional glass-ionomer cements commonly used for stainless steel crowns cementation might be of interest for clinical application as luting agent for CAD/CAM RC crowns. The analyses of the microtensile bond strength test to evaluate bonding performance to dentin, detected no significant differences among EB-Cem, EB-CX, and HC-Cem.
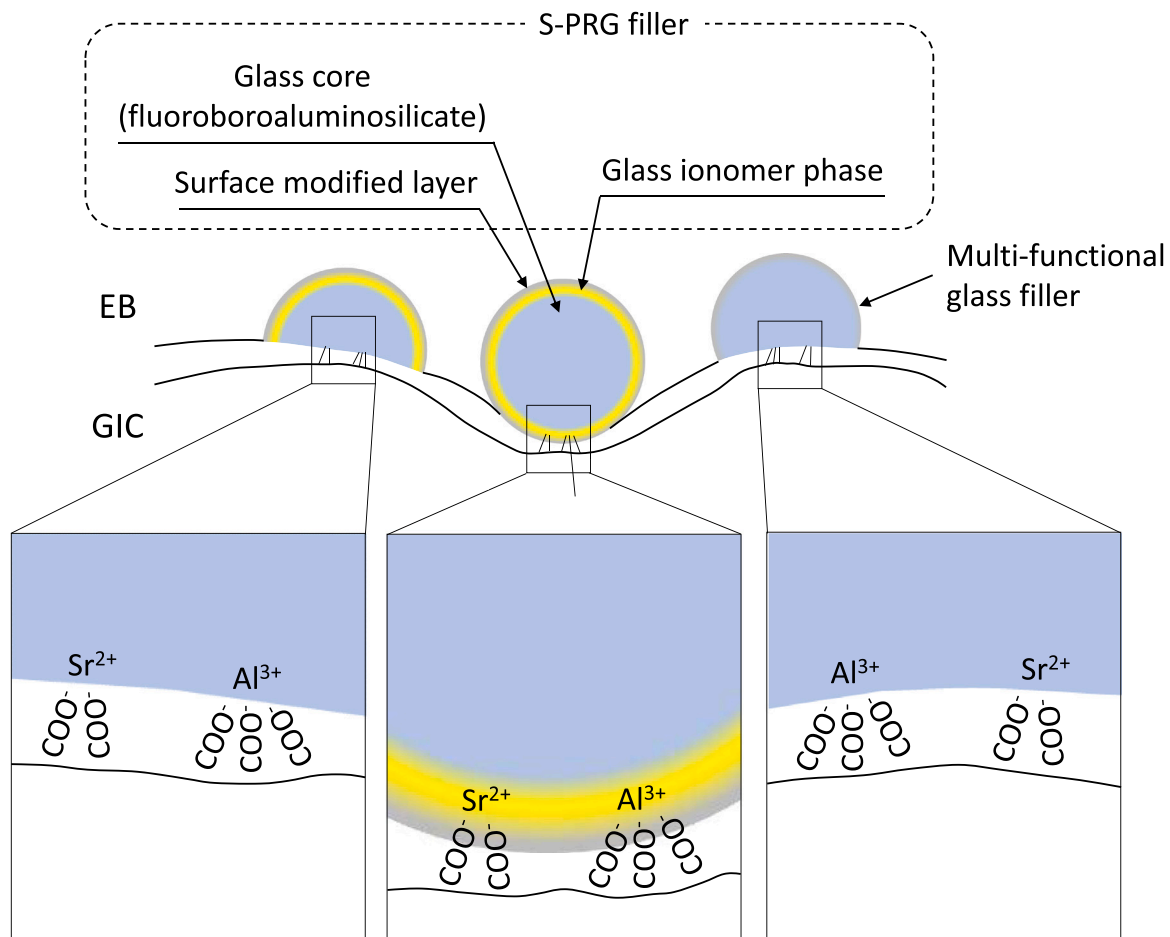
Fig. 6. Schematic illustration of adhesion via the ionic/coordinate bond between Sr^{2+}/Al^{3+} on the surface pre-reacted glass filler, which is exposed on the inner surface of the computer-aided design/computer-aided manufacturing resin composite crown, and the carboxylate ions in the polyacrylic acid of the conventional glass-ionomer cement.

Regarding EB-CX, the mixed fractures were observed after the microtensile bond strength test between CAD/CAM RC and CX. Also, remnants of the cement were observed on the inner surface of CAD/CAM RC crowns similar to EB-Cem and HC-Cem. Conventional glass-ionomer cements set via the acid-base reaction between polyacrylic acid and the cations (Ca^{2+} and Al^{3+}) that eluted from the aluminosilicate glasses. It is also known that they chemically bond with Ca of the tooth substrate or metals. The S-PRG filler is produced by grinding an acid reactive fluoroboroaluminosilicate glass, followed by a surface treatment, and spraying polyacrylic acid to form a stable glass-ionomer layer containing F^-, Al^{3+}, BO_3^{3-}, Na^+, SiO_4^{4-}, or Sr^{2+} on its surface. There was no significant difference in the microtensile bond strengths between EB-Cem and EB-CX. It is likely that the S-PRG filler-incorporated EB achieved adhesion via the ionic/coordinate bond between Sr^{2+}/$Al^3{}^+$ on the S-PRG filler, which is exposed on the inner surface of the CAD/CAM RC crown, and the carboxylate ions in the polyacrylic acid of CX`s liquid (Fig. 6). In fact, the greater fracture load of EB-CX regarding HC-CX in the single load to failure and microtensile bond strength tests suggests that the CAD/CAM RC crown incorporating S-PRG filler successfully adhered to the CX as expected.

The Weibull configuration factor β, the performance of all the specimens was mainly accelerated by materials strength rather than fatigue damage as the cycles elapsed (β < 1) [12–16]. The Weibull modulus m, a unitless parameter used to describe the variation in strength values and structural reliability as a result of flaw populations [4,16,17], for

EB-Cem and EB-CX was significantly greater than that of HC-Cem and HC-CX. This suggests that EB has good structural reliability regardless of whether resin cement or CX is used under cyclic loading condition. The scale parameter η indicates the fatigue load-at-failure of the CAD/CAM RC crowns. Significantly higher η values were observed for EB-Cem and HC-Cem when compared with EB-CX and HC-CX. This finding suggests that the bonding ability of resin cement is higher than that of CX. On the other hand, EB-CX presented the lowest eta among all groups (812.83 CI: 740.31–892.45), and it was close to 814 N, which is the mean occlusal load in adult males [11], and greater than 155 N, which is the mean occlusal load in children aged six to 18 years old [18]. These results suggest that EB has clinically acceptable fatigue behavior for restoring primary molar teeth even when the CX is used. While significantly higher reliability was observed for EB independent on the cementation material, further clinical studies are required to demonstrate the clinical performance of the CAD/CAM RC crowns for primary teeth.

Furthermore, the S-PRG filler exhibits a sustained-release of multiple ions: F^-, Al^{3+}, BO_3^{3-}, Na^+, SiO_4^{4-}, or Sr^{2+} [5]. RCs incorporating the S-PRG filler inhibit proliferation of *Streptococcus mutans* by releasing BO_3^{3-} and F^- [19,20]. The downregulation of carbohydrate metabolism of *S. mutans* has been associated with the inhibition of plaque adhesion to the surface of RCs incorporating S-PRG filler [21–24], and improvement of acid resistance and remineralization functions [25,26]. Therefore, the use of CAD/CAM RC crowns

incorporating S-PRG fillers is expected to prevent secondary caries and enamel demineralization of proximal teeth. These benefits must be investigated in further studies.

5. Conclusions

The crowns fabricated with the experimental CAD/CAM RC incorporating S-PRG filler yielded greater fracture loads and reliability than the crowns manufactured with commercially available CAD/CAM RC regardless of the luting materials. These findings suggest that the experimental CAD/CAM RC crown may be clinically useful for the restoration of primary molars.

Acknowledgements

Appendix A. Supporting information

Supplementary data associated with this article can be found in the online version at doi:10.1016/j.dental.2023.04.006.

References

[1] Dye BA, Tan S, Smith V, Lewis BG, Barker LK, Thornton-Evans G, et al. Trends in oral health status: United States 1988-1994 and 1999-2004. Vital Health Stat 2007;11:1–92.

[2] Roberts JF, Sherriff M. The fate and survival of amalgam and preformed crown molar restorations placed in a specialist paediatric dental practice. Br Dent J 1990;169:237–44.

[3] Nakase Y, Yamaguchi S, Okawa R, Nakano K, Kitagawa H, Imazato S. Physical properties and wear behavior of CAD/CAM resin composite blocks containing S-PRG filler for restoring primary molar teeth. Dent Mater Publ Acad Dent Mater 2022;38:158–68.

[4] Bonfante EA, Coelho PG. A critical perspective on mechanical testing of implants and prostheses. Adv Dent Res 2016;28:18–27.

[5] Imazato S, Kohno T, Tsuboi R, Thongthai P, Xu HH, Kitagawa H. Cutting-edge filler technologies to release bio-active components for restorative and preventive dentistry. Dent Mater J 2020;39:69–79.

[6] Yamaguchi S, Kani R, Kawakami K, Tsuji M, Inoue S, Lee C, et al. Fatigue behavior and crack initiation of CAD/CAM resin composite molar crowns. Dent Mater Publ Acad Dent Mater 2018;34:1578–84.

[7] Madlena M, Keszthelyi G, Alberth M, Nagy A. [The attrition of deciduous teeth]. Fogorv Sz 1989;82:273–6.

[8] Seligman DA, Pullinger AG, Solberg WK. The prevalence of dental attrition and its association with factors of age gender occlusion and TMJ symptomatology. J Dent Res 1988;67:1323–33.

[9] Lee C, Yamaguchi S, Imazato S. Quantitative evaluation of the degradation amount of the silane coupling layer of computer-aided design/computer-aided manufacturing resin composites by water absorption. J Prosthodont Res 2021.

[10] Karaer O, Yamaguchi S, Nakase Y, Lee C, Imazato S. In silico non-linear dynamic analysis reflecting in vitro physical properties of CAD/CAM resin composite blocks. J Mech Behav Biomed Mater 2020;104:103697.

[11] Braun S, Bantleon HP, Hnat WP, Freudenthaler JW, Marcotte MR, Johnson BE. A study of bite force.2. relationship to various cephalometric measurements. Angle Orthod 1995;65:373–7.

[12] Bonfante EA, Suzuki M, Carvalho RM, Hirata R, Lubelski W, Bonfante G, et al. Digitally produced fiber-reinforced composite substructures for three-unit implant-supported fixed dental prostheses. Int J Oral Maxillofac Implants 2015;30:321–9.

[13] Bonfante EA, Suzuki M, Hirata R, Bonfante G, Fardin VP, Coelho PG. Resin composite repair for implant-supported crowns. J Biomed Mater Res B Appl Biomater 2017;105:1481–9.

[14] Bonfante EA, Suzuki M, Lorenzoni FC, Sena LA, Hirata R, Bonfante G, et al. Probability of survival of implant-supported metal ceramic and CAD/CAM resin nanoceramic crowns. Dent Mater Publ Acad Dent Mater 2015;31:e168–77.

[15] Bonfante EA, Coelho PG, Navarro Jr. JM, Pegoraro LF, Bonfante G, Thompson VP, et al. Reliability and failure modes of implant-supported Y-TZP and MCR three-unit bridges. Clin Implant Dent Relat Res 2010;12:235–43.

[16] Zhao WB, Elsayed EA. A general accelerated life model for step-stress testing. Iie Trans 2005;37:1059–69.

[17] Tinschert J, Zwez D, Marx R, Anusavice KJ. Structural reliability of alumina feldspar leucite mica and zirconia-based ceramics. J Dent 2000;28:529–35.

[18] Verkouteren DRC, de Sonnaville WFC, Zuithoff NPA, Wulffraat NM, Steenks MH, Rosenberg A. Growth curves for mandibular range of motion and maximum voluntary bite force in healthy children. Eur J Oral Sci 2022;130:e12869.

[19] Miki S, Kitagawa H, Kitagawa R, Kiba W, Hayashi M, Imazato S. Antibacterial activity of resin composites containing surface pre-reacted glass-ionomer (S-PRG) filler. Dent Mater Publ Acad Dent Mater 2016;32:1095–102.

[20] Kitagawa H, Miki-Oka S, Mayanagi G, Abiko Y, Takahashi N, Imazato S. Inhibitory effect of resin composite containing S-PRG filler on streptococcus mutans glucose metabolism. J Dent 2018;70:92–6.

[21] Saku S, Kotake H, Scougall-Vilchis RJ, Ohashi S, Hotta M, Horiuchi S, et al. Antibacterial activity of composite resin with glass-ionomer filler particles. Dent Mater J 2010;29:193–8.

[22] Nomura R, Morita Y, Matayoshi S, Nakano K. Inhibitory effect of surface pre-reacted glass-ionomer (S-PRG) eluate against adhesion and colonization by streptococcus mutans. Sci Rep 2018;8:5056.

[23] Zeng L, Das S, Burne RA. Utilization of lactose and galactose by streptococcus mutans: transport toxicity and carbon catabolite repression. J Bacteriol 2010;192:2434–44.

[24] Busuioc M, Buttaro BA, Piggot PJ. The pdh operon is expressed in a subpopulation of stationary-phase bacteria and is important for survival of sugar-starved streptococcus mutans. J Bacteriol 2010;192:4395–402.

[25] Uo M, Wada T, Asakura K. Structural analysis of strontium in human teeth treated with surface pre-reacted glass-ionomer filler eluate by using extended X-ray absorption fine structure analysis. Dent Mater J 2017;36:214–21.

[26] Ito S, Iijima M, Hashimoto M, Tsukamoto N, Mizoguchi I, Saito T. Effects of surface pre-reacted glass-ionomer fillers on mineral induction by phosphoprotein. J Dent 2011;39:72–9.